

Taming the single-cylinder scattering through time-modulation - The role of the modulation phase

J. Yan,^{1,*} I. Katsantonis,^{1,2} M. Mostafa,³ V. Asadchy,³ and M. Kafesaki^{1,2,†}

¹*Institute of Electronic Structure and Laser,
Foundation for Research and Technology-Hellas, 70013 Heraklion, Crete, Greece*

²*Department of Materials Science and Technology,
University of Crete, 70013 Heraklion, Crete, Greece*

³*Department of Electronics and Nanoengineering,
School of Electrical Engineering, Aalto University, 02150 Espoo, Finland*

Abstract

Dielectric particles with time-modulated electromagnetic properties exhibit intriguing scattering phenomena, entailing unique response and possibilities in meta-structures made of such particles. In this work, we investigate the scattering properties of an infinitely-long cylinder with periodically time-modulated permittivity. We demonstrate parametric scattering amplification, depending on the strength of the modulation, as well as controllable angular scattering pattern, ranging from enhanced forward to enhanced backward, or even scattering cancellation. This angular tunability is achieved through appropriate control of the modulation phase, highlighting its critical role in multi-modal time-modulated scattering systems.

I. INTRODUCTION

Time-varying media provide an additional degree of freedom for tailoring wave-matter interactions, enabling novel effects and functionalities, unachievable in static media [1–11]. The temporal modulation, in the form of temporal interfaces where a dispersionless medium undergoes sudden changes in material properties, has been first analyzed by Morgenthaler in 1958 [12]. Morgenthaler showed that the temporal boundary conditions imply conservation of the wavevector, and that temporal reflection and frequency conversion of incident waves arise. The expanding interest, though, in the study of time-modulated media has emerged more recently, largely driven by advances in photonic crystals and metamaterials, which have highlighted the vast potential of engineered spatial variations. Extending this paradigm to the temporal domain has opened new ways for wave manipulation. Temporal boundaries, in particular, have enabled a variety of applications, including temporal aiming [5], anti-reflection temporal coatings [13], extension in the bandwidth of absorbers [14], as well as broadband amplification of light [15].

On the other hand, if the material properties of a medium vary periodically in time, momentum bandgaps are formed [16], in analogy to the frequency bandgaps of conventional photonic crystals with spatial periodicity. Such systems are thus referred to as the photonic time crystals (PTCs). Due to the temporal periodicity, Floquet theorem is applicable to

* jiaruo.yan@iesl.forth.gr

† kafesaki@iesl.forth.gr

PTC [2], providing a rigorous framework for analyzing and understanding wave propagation in these media. Within the momentum bandgaps of PTC, two modes with imaginary frequencies are supported by Maxwell’s equations. These correspond to two eigenmodes: one that decays and one that grows exponentially in time. Notably, unlike in spatially periodic systems, the amplifying mode is physically allowed, reflecting the non-conservative nature of time-modulated media and their ability to exchange energy with the modulation. Recent studies have shown that structural resonances can expand the momentum bandgap relative to that of a homogeneous bulk medium, for the same modulation strength [17, 18]. (Note that amplification in PTCs, unlike the conventional parametric amplification, is not essentially a resonance-requiring process[19].)

Structural resonances can be implemented in various ways, e.g. using metasurfaces. In the context of time-modulated Floquet metasurfaces, analytical approaches based on equivalent circuit approaches [20, 21], transition matrix approach [22], and homogenization techniques based on generalized transition sheet conditions or surface susceptibilities [23, 24] have been developed and validated with numerical results. Applications including frequency conversion [25–27], parametric amplification [28, 29], electromagnetic absorption [20, 30], subwavelength imaging [21], and nonreciprocal responses [31–33] have been reported.

A conceptually easy approach to realize resonant Floquet metasurfaces, in particular in the near-IR and optical region, is the involvement of dielectric scatterers supporting Mie resonances. In this context, scattering particles of spherical [34–36] and extended shapes [37], have been investigated under periodic temporal modulation of their relative permittivity, considering cases with and without intrinsic frequency dispersion. Quasi-bound states in continuum (quasi-BIC) resonances hosted in metasurfaces formed by spherical scatterers have been shown to lower the minimum modulation strength required to achieve lasing and coherent absorption [38]. Reference [39] also discussed quasi-BIC states sustained in time-modulated metasurfaces composed of multilayered spheres, demonstrating their effectiveness in reducing the modulation strength required to realize wide momentum bandgaps.

Despite the extensive body of work on metasurfaces based on spherical scatterers, time-modulated metasurfaces composed of cylindrical Mie resonators remain largely unexplored. Such structures are realizable, for example, employing plasma tubes at microwave frequencies, or semiconducting or transparent conductive oxide wires at higher frequencies. Combining resonant responses with inherent anisotropy, these structures offer a promising platform

for accessing additional and currently unexplored wave phenomena.

In this work, we take a first step in the direction of time-modulated cylinder-based metasurfaces, by investigating their fundamental building block, i.e. an infinitely long cylinder with periodically time-modulated permittivity. Although a cylinder of infinite length cannot be fabricated in practice, we expect our theoretical framework to be well applicable to cylinders of lengths that are finite but much longer than the operational wavelengths. Our study not only demonstrates the emergence of strong parametric resonances in the time-modulated cylinder, but also reveals the critical role of the modulation phase in the cylinder scattering response. We show that by appropriately tuning the modulation phase the scattered field can be controlled in the angular distribution, enabling even transitions from enhanced forward to enhanced backward scattering. This behavior is expected to be a general feature of multi-mode systems, since the modulation phase is shown to govern the interference among the different harmonics arising from time-modulation, in addition to the simultaneously excited Mie resonant modes. Thus, our results propose modulation phase engineering as a key mechanism for controlling wave scattering, opening new avenues for the design of time-varying metasurfaces.

The rest of the paper is structured as follows: In Section II, we establish the theoretical framework for the single-cylinder scattering problem using Floquet–Mie theory, and derive analytical expressions for the scattered fields as well as the corresponding scattering efficiencies. Section III examines the conditions for parametric resonances, in terms of the modulation frequency and modulation strength; their relationship to the conventional Mie resonances is also discussed. Through the interference between the scattered harmonics associated with different multipolar modes, we demonstrate how the far-field radiation can be engineered in Section IV. We explore the additional degrees of freedom provided by negative-frequency scattered components, and by the harmonic phase shifts induced by the time-modulation. We show that, by properly selecting the modulation parameters to simultaneously excite multipoles of different orders and by controlling the modulation phase, distinct radiation patterns can be achieved at the same input frequency.

II. FORMALISM

We consider a single infinitely long cylinder of material with relative permittivity ε_r and permeability μ_r , embedded in a homogeneous host medium of relative permittivity ε_h and permeability μ_h . Assuming a simple temporal variation of the relative permittivity of the cylinder in the sinusoidal form, and expanding it in Fourier series we have

$$\varepsilon_r(t) = \varepsilon_{r0} + \Delta\varepsilon \cos(2\pi f_m t + \beta) = \sum_{n=-N}^N \varepsilon(n) \exp(in2\pi f_m t), \quad (1)$$

where ε_{r0} is the static permittivity, i.e. the permittivity in the absence of time-modulation, β is the modulation phase, $\Delta\varepsilon$ is the modulation strength, $\varepsilon(n)$ are the Fourier coefficients in the expansion, and $f_m = 1/T_m$ is the modulation frequency. To solve the scattering problem for such a time-modulated cylinder, the first step is to find the allowed solutions of the wave equation inside the cylinder.

Applying the Floquet theorem to the electric and magnetic fields ($\mathbf{E}(\mathbf{r}, t)$ and $\mathbf{H}(\mathbf{r}, t)$ respectively), and expanding the periodic amplitudes into a Fourier series as in Eq. (1), we obtain $\mathbf{F}(\mathbf{r}, t) = \sum_{n=-N}^N \mathbf{F}^{(n)}(\mathbf{r}) \exp[-i2\pi f^{(n)}t]$ ($\mathbf{F} = \mathbf{E}$ or \mathbf{H}), where $f^{(n)} = f - nf_m$ is the n -th frequency harmonic supported by the time-modulated medium. Substituting the electric field and the permittivity of Eq. (1) into the wave equation, we obtain

$$\nabla^2 \mathbf{E}(t) = \frac{\mu_h}{c^2} \frac{\partial^2 \varepsilon_r(t) \mathbf{E}(t)}{\partial t^2}, \quad (2)$$

and taking into account that in a homogeneous medium $\nabla^2 \mathbf{E} = -q^2 \mathbf{E}$ with q being the wave number in the medium, we obtain [16, 34]

$$\mu_h \left(2\pi \frac{f - nf_m}{c}\right)^2 \sum_{p=-N}^N \varepsilon(n-p) \mathbf{E}^{(p)} = q^2 \mathbf{E}^{(n)}, \quad (3)$$

where p is an integer. Eq. (3) is essentially an eigenvalue problem of the form

$$\underline{D} \underline{M} \mathbf{v} = q^2 \mathbf{v}, \quad (4)$$

where \underline{D} is a diagonal matrix with elements $D_{n',n'} = \mu_h [2\pi(f - nf_m)]^2 / c^2$ (with $n' = n + N + 1$ to denote the matrix element indices), and \underline{M} is formed by the Fourier coefficients from Eq (1), as $M_{n',p'} = \varepsilon(n-p)$, with $n, p = -N, -N+1, \dots, N$, $p' = p + N + 1$ as matrix element indices. Solving the problem above, we obtain for a time-modulated infinite medium $2N + 1$ eigenvalues, q_p^2 (squares of the allowed wavenumbers), $p = -N, \dots, N$, as well as $2N + 1$

eigenvectors, \mathbf{v}_p (considered here normalized to unity, with further discussions regarding the normalization in Appendix B), each containing $2N + 1$ elements, $v_p(n)$ ($v_p(n)$ is the electric field amplitude of the Fourier harmonic with order n contained in the eigenvector \mathbf{v}_p) [34].

Solving the above eigenvalue problem we can identify the eigenvalues and eigenvectors of the time-modulated medium, and thus express the fields in terms of them. In our case, where the system of interest is a cylinder, it is convenient to express the fields, in and out of the cylinder, in the basis of cylindrical vector harmonics.

Taking the TE polarization as an example, i.e. \mathbf{E} field perpendicular to the cylinder axis (illustrated on the right side of Fig. 1(a)), and considering a normally incident (with respect to the cylinder axis) plane wave of frequency f , the field outside the cylinder (sum of the incident and scattered fields) can be expressed as (taking into account that the cylinder will generate fields of frequencies $f^{(n)} = f - nf_m$; see text after Eq. (1)),

$$\mathbf{E}_h(\mathbf{r}, t) = \sum_{n=-N}^N \mathbf{E}_h^{(n)}(\mathbf{r}) \exp[-i2\pi(f - nf_m)t] \quad (5)$$

with $\mathbf{E}_h^{(n)}(\mathbf{r}) = \mathbf{E}_{inc}(\mathbf{r})\delta_{n0} + \mathbf{E}_{sc}^{(n)}(\mathbf{r}) = i \sum_{l=0}^{\infty} \left[a_l^0 \mathbf{m}_l(k_0, \mathbf{r})\delta_{n0} + a_{l+}^{(n)'} \mathbf{m}'_l(q_{hn}, \mathbf{r}) \right],$

where the subscript h represents the host medium, \mathbf{m}_l is the l -th order vector cylindrical harmonic \mathbf{m} (see Appendix A) expressed in terms of Bessel functions, and \mathbf{m}'_l is expressed by replacing the Bessel functions by the corresponding Hankel functions, representing scattered outgoing cylindrical waves. $a_l^0, a_{l+}^{(n)'}$ are the expansion coefficients of the incident (0-th Fourier harmonic) and the scattered (n -th Fourier harmonic) fields, respectively. Assuming homogeneous host medium, $k_0 = \sqrt{\varepsilon_h \mu_h} (2\pi f/c)$ is the wave number of the incident wave, and $q_{hn} = \sqrt{\varepsilon_h \mu_h} (2\pi(f - nf_m)/c)$ is the wave number of the scattered n -th Fourier harmonic. Similarly, the field inside the cylinder can be written as

$$\mathbf{E}_c(\mathbf{r}, t) = \sum_{n=-N}^N \mathbf{E}_c^{(n)}(\mathbf{r}) \exp[-i2\pi(f - nf_m)t] \quad (6)$$

with $\mathbf{E}_c^{(n)}(\mathbf{r}) = i \sum_{p=-N}^N v_p(n) \sum_l a'_{l;p} \mathbf{m}_l(q_p, \mathbf{r}),$

where $a'_{l;p}$ is the l -th cylindrical harmonic expansion coefficient of the p -th eigenmode within the time-modulated cylinder, and $v_p(n)$ is the element of the eigenvector \mathbf{v}_p . Analogously,

we obtain the expressions for the magnetic field, \mathbf{H} , as follows:

$$\mathbf{H}_c(\mathbf{r}, t) = \sum_{n=-N}^N \mathbf{H}_c^{(n)}(\mathbf{r}) \exp[-i2\pi(f - nf_m)t] \quad (7)$$

$$\text{with } \mathbf{H}_c^{(n)}(\mathbf{r}) = \sum_{p=-N}^N v_p(n) \sum_l b'_{l;p} \mathbf{n}_l(q_p, \mathbf{r}).$$

(In the above equations \mathbf{n}_l is the l -th order vector cylindrical harmonic \mathbf{n} - see Appendix A.) Applying the boundary conditions equating the tangential components of the electric fields \mathbf{E} and magnetic fields \mathbf{H} , one can obtain, for each n and l ,

$$\sum_{p=-N}^N a_{l;p} v_p(n) \frac{\partial J_l(q_p R)}{\partial (q_p R)} = \frac{\partial J_l(k_0 R)}{\partial (k_0 R)} \delta_{n0} + a_{l+}^{(n)} \frac{\partial H_l(q_{hn} R)}{\partial (q_{hn} R)}, \quad (8)$$

$$\sum_{p=-N}^N b_{l;p} v_p(n) J_l(q_p R) = J_l(k_0 R) \delta_{n0} + b_{l+}^{(n)} H_l(q_{hn} R), \quad (9)$$

where R is the radius of the cylinder, J_l, H_l are the l -th order Bessel function and Hankel function respectively. The scattering coefficients $a_{l;p}, b_{l;p}$ and $a_{l+}^{(n)}, b_{l+}^{(n)}$ are all normalized to that of the input wave (e.g. $a_{l+}^{(n)} = a_{l+}^{(n)'} / a_l^0$ from Eq. (2)). In addition, we have the relationships: $q_p a_{l;p} = b_{l;p} \mu_r 2\pi(f - nf_m) / c$, $a_l^0 = \sqrt{\mu_h / \varepsilon_h} b_l^0$ and $a_{l+}^{(n)} = \sqrt{\mu_h / \varepsilon_h} b_{l+}^{(n)}$. (For host medium (e.g. air) with $\varepsilon_h = \mu_h = 1$ specifically, the scattering coefficients $a_{l+}^{(n)} = b_{l+}^{(n)}$ are interchangeable for a certain polarization. We solve for $a_{l+}^{(n)}$ in the TE case, and $b_{l+}^{(n)}$ in the TM case and use the corresponding coefficients for later definitions, in order to distinguish the TE and TM cases.) Therefore, there are essentially $2(2N + 1)$ parameters ($a_{l;p}$, and $a_{l+}^{(n)}$, $n, p = -N, -N + 1 \dots N$), numerically solvable based on the above set of simultaneous equations.

The expressions for the TM case can be obtained in a similar way (see Appendix A), and are as follows:

$$\sum_{p=-N}^N a_{l;p} v_p(n) J_l(q_p R) = J_l(k_0 R) \delta_{n0} + a_{l+}^{(n)} H_l(q_{hn} R), \quad (10)$$

$$\sum_{p=-N}^N b_{l;p} v_p(n) \frac{\partial J_l(q_p R)}{\partial (q_p R)} = \frac{\partial J_l(k_0 R)}{\partial (k_0 R)} \delta_{n0} + b_{l+}^{(n)} \frac{\partial H_l(q_{hn} R)}{\partial (q_{hn} R)}. \quad (11)$$

Thereby we obtained the coefficients, for the TE ($a_{l+}^{(n)}$ from Eqs. (8) and (9)), or for the TM case ($b_{l+}^{(n)}$ from Eqs. (10) and (11)). We define the total scattering efficiency for the TE mode, the summation of the contributions from all the harmonics taken into account in the

calculations as (similar to the definition for a spherical particle in [34])

$$Q_{sc} = \sum_{n=-N}^N Q^{(n)} = \sum_{n=-N}^N \frac{2}{|q_{hn}|R} \sum_l \frac{2}{1 + \delta_{l0}} |a_{l+}^{(n)}|^2. \quad (12)$$

For the TM mode, the scattering efficiency is defined by replacing $a_{l+}^{(n)}$ with $b_{l+}^{(n)}$ in Eq. (12). If $N = 0$, the above formalism reduces to the problem of scattering from a time-invariant infinite cylinder [40].

III. PARAMETRIC MIE RESONANCES

The scattering efficiencies for TE and TM incident waves, of a static dielectric cylindrical scatterer with $R = 5$ mm, $\varepsilon_r = 12$, are plotted as the black dashed curves in Fig. 1, referenced to the right axes, from which we identify the corresponding Mie resonances. Given an incident frequency f , modulating the relative permittivity at a $f_m = 2f$, following the modulation form stated in Eq. (1), parametric resonances can be realized, where the scattering efficiencies are amplified significantly. The conditions for the parametric resonances can be established based on Eqs. (8-11) for the eigen-modes, where the resonances occur without incident fields. The dominant harmonics of time-modulated cylinders showing parametric resonances are the $n = 0$ and $n = 1$ modes, if the modulation frequency is twice the input frequency, $f_m = 2f$. The fundamental scattering mode ($n = 0$) is of $f^{(0)} = f$, and $n = 1$ is the corresponding negative-frequency mode $f^{(1)} = -f$, which represents backward propagating waves.

With the modulated relative permittivity taking the form as in Eq. (1), the eigenvalues (supported wave vectors within the modulated cylinder) can be obtained as $q_{p=0,1} = (2\pi f/c) \sqrt{\varepsilon_{r0} \pm \Delta\varepsilon/2}$ (details can be found in the Appendix B). The respective eigenvectors are $\mathbf{v}_{p=0,1} = [1; \pm e^{i\beta}]$.

The truncated eigen-problem as discussed in [36] (for spherical scatterers), taking into

account only the dominant harmonics ($n = 0, 1$), for the TE mode, can be written as

$$\begin{pmatrix} -\frac{\partial J_l(q_{p=1}R)}{\partial(q_{p=1}R)} e^{i\beta} & \frac{\partial J_l(q_{p=0}R)}{\partial(q_{p=0}R)} e^{i\beta} & -\frac{\partial H_l(q_{h1}R)}{\partial(q_{h1}R)} & 0 \\ \frac{\partial J_l(q_{p=1}R)}{\partial(q_{p=1}R)} & \frac{\partial J_l(q_{p=0}R)}{\partial(q_{p=0}R)} & 0 & -\frac{\partial H_l(q_{h0}R)}{\partial(q_{h0}R)} \\ -q_{p=1} J_l(q_{p=1}R) e^{i\beta} & q_{p=0} J_l(q_{p=0}R) e^{i\beta} & -\mu_r q_{h1} H_l(q_{h1}R) & 0 \\ q_{p=1} J_l(q_{p=1}R) & q_{p=0} J_l(q_{p=0}R) & 0 & -\mu_r q_{h0} H_l(q_{h0}R) \end{pmatrix} \cdot \begin{pmatrix} a_{l;p=1} \\ a_{l;p=0} \\ a_{l+}^{(1)} \\ a_{l+}^{(0)} \end{pmatrix} = \mathbf{0} \quad (13)$$

where the Bessel and Hankel (J_l , H_l) functions, and $q_{h0} = 2\pi f/c = -q_{h1}$ are as described in Section II. $a_{l;p=0}$ and $a_{l;p=1}$ are the scattering coefficients within the cylinder, corresponding to the two eigenmodes described by $q_{p=0,1}$ and $\mathbf{v}_{p=0,1}$. Note that the modulation phase induces a phase delay in the scattering coefficient of order $n = 1$, i.e. $a_{l+}^{(1)}$. Further discussions regarding the phase induced by time-modulation are given in Section IV. The TM mode eigen-problem then follows as,

$$\begin{pmatrix} -\frac{\mu_r q_{h1}}{q_{p=1}} J_l(q_{p=1}R) e^{i\beta} & \frac{\mu_r q_{h1}}{q_{p=0}} J_l(q_{p=0}R) e^{i\beta} & -H_l(q_{h1}R) & 0 \\ \frac{\mu_r q_{h0}}{q_{p=1}} J_l(q_{p=1}R) & \frac{\mu_r q_{h0}}{q_{p=0}} J_l(q_{p=0}R) & 0 & -H_l(q_{h0}R) \\ -\frac{\partial J_l(q_{p=1}R)}{\partial(q_{p=1}R)} e^{i\beta} & \frac{\partial J_l(q_{p=0}R)}{\partial(q_{p=0}R)} e^{i\beta} & -\frac{\partial H_l(q_{h1}R)}{\partial(q_{h1}R)} & 0 \\ \frac{\partial J_l(q_{p=1}R)}{\partial(q_{p=1}R)} & \frac{\partial J_l(q_{p=0}R)}{\partial(q_{p=0}R)} & 0 & -\frac{\partial H_l(q_{h0}R)}{\partial(q_{h0}R)} \end{pmatrix} \cdot \begin{pmatrix} b_{l;p=1} \\ b_{l;p=0} \\ b_{l+}^{(1)} \\ b_{l+}^{(0)} \end{pmatrix} = \begin{pmatrix} 0 \\ 0 \\ 0 \\ 0 \end{pmatrix}. \quad (14)$$

In order to obtain eigen-solutions of the scattering coefficients that are non-zero, we set the determinant of the above 4×4 matrices on the left hand side to zero. This then leads to the approximate conditions for parametric resonances. The eigen-problem is solved for TE and TM modes, for each multipolar mode l separately, and the results are plotted in Fig. 1. The horizontal axis is the incident frequency f , and the modulation frequency f_m is varied for each f to be $f_m = 2f$, as required for achieving parametric conditions. The calculated threshold modulation strengths are referenced to the left axes in log-scale, $\log_{10}(\Delta\varepsilon_{th}/\varepsilon_{r0})$. The solid curves of different colors represent results of different multipolar order l .

In addition, we show in Fig. 1(a) (dots) the results of $\Delta\varepsilon_{th}$ taking into account more frequency harmonics. Here the threshold modulation strengths were determined by maximizing the Q_{sc} (as defined in Eq. (12)) to obtain the data in dots, taking into account more harmonics ($N = 3$, seven harmonics in total). While truncated eigen-problem is a better approximation for weaker modulations, in cases of stronger modulations, higher-order harmonics are non-negligible. Differences between the results obtained by the two meth-

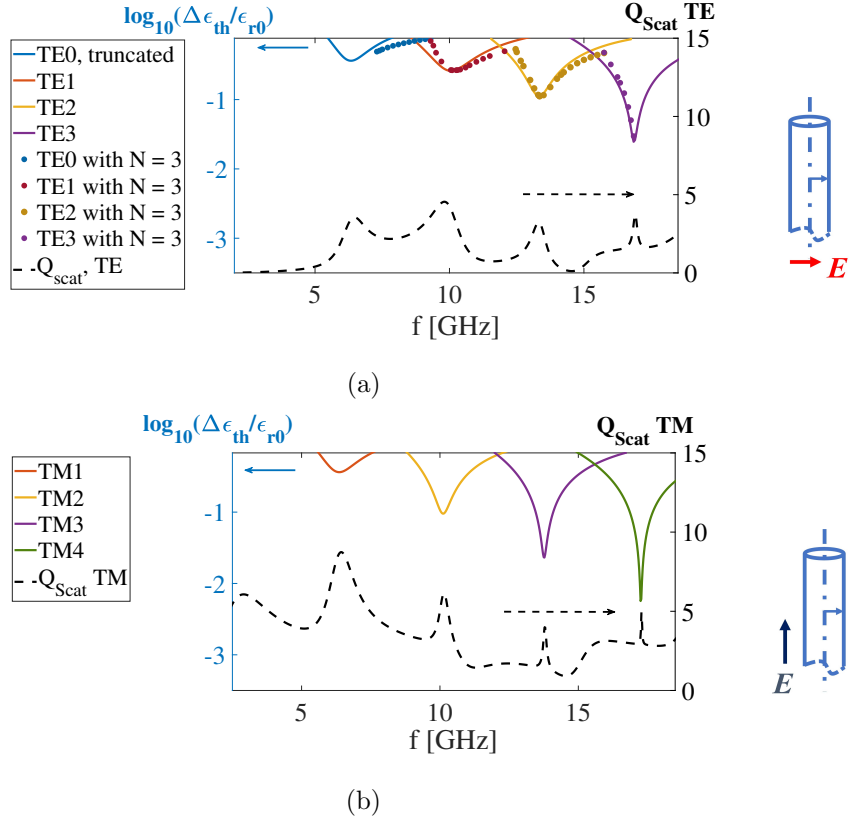


FIG. 1: Threshold values of the modulation strengths $\Delta\epsilon_{th}$ required for parametric resonances ($\epsilon_{r0} = 12$, $R = 5$ mm, modulation frequency always satisfies $f_m = 2f$, colored solid curves, left axes), and scattering efficiencies of cylinders with static relative permittivity $\epsilon_r = 12$ (black dashed curve, right axes). (a) TE mode, where the solid curves are $\log_{10}(\Delta\epsilon_{th}/\epsilon_{r0})$ based on the truncated eigenvalue problem in Eq. (13), and the dots are results based on Eqs. (8) and (9) from Section 2, taking into account higher-order harmonics. (b) TM mode, results of $\Delta\epsilon_{th}$ based on Eq. (14). The minimum threshold modulation strengths for each multipolar mode occur at the Mie resonant frequencies of the static system.

ods (dots and solid curves of the corresponding color) can be seen in Fig. 1(a), especially for cases where larger $\Delta\epsilon$ values are required. Similar deviations of the threshold modulation strengths from those obtained via the truncated eigen-problem were discussed in the supplementary of [36] where 24 harmonics were taken into account.

The minima of the threshold modulation strengths for each mode occur at f (with $f_m = 2f$) close to the corresponding Mie resonances of an unmodulated cylinder of ϵ_{r0} ,

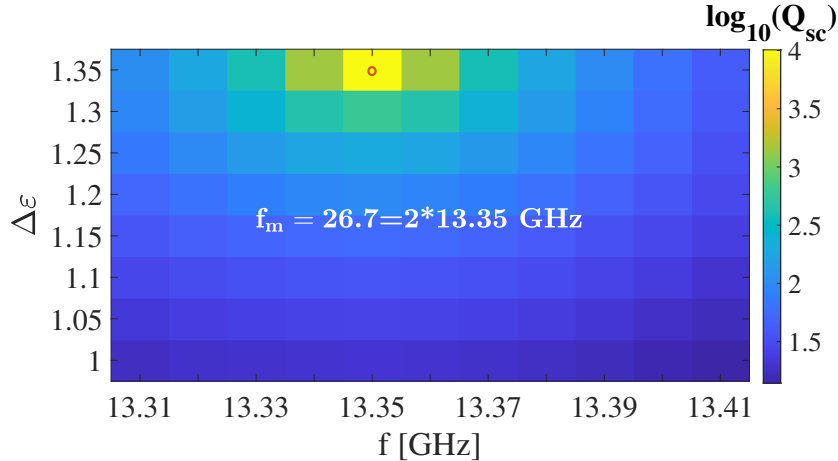


FIG. 2: Total scattering efficiency as defined in Eq. (12), TE mode, plot in color and in log-scale, $\log_{10}(Q_{sc})$. Modulation frequency is $f_m = 26.7$ GHz. x -axis is incident frequency f , y -axis is the modulation strength $\Delta\epsilon$. At $\Delta\epsilon = 1.35$, which is also very close to the calculated threshold value as in Fig. 1(a), Q_{sc} reaches a maximum at

$$f = f_m/2 = 13.35 \text{ GHz.}$$

demonstrated by the alignments between the dips of the solid curves and the peaks of the dashed curves in Fig. 1. As discussed in detail in Appendix C, the minimum values of the threshold modulation strengths are dependent on the quality factors of the respective Mie resonances for the static system. It should also be noted here that the scattering properties of the unmodulated case are scalable over frequency, dependent on the electrical size of the scatterer. The frequency scalability also applies to the eigen-solutions for obtaining the threshold modulation strengths.

Figure 2 is a color plot of the total scattering efficiency based on Eq. (12), shown in logarithmic scale with base 10. The horizontal axis is the frequency of incident plane wave f in the calculations, and the vertical axis is the varying modulation strength, $\Delta\epsilon$. With a modulation frequency fixed at $f_m = 26.7$ GHz, at half of the modulation frequency, $f = f_m/2$, the Q_{sc} reaches a maximum when $\Delta\epsilon = 1.35$, which is very close to the threshold modulation strength as shown in Fig. 1(a). Above the threshold modulation strength, the scattering efficiency diverges at $f = 13.35$ GHz since we are at the regime of parametric oscillations. In practical experiments, it will saturate after reaching certain high values due to the nonlinearity when the fields become very strong, and thus detuning the linear system from ideal conditions of parametric oscillations.

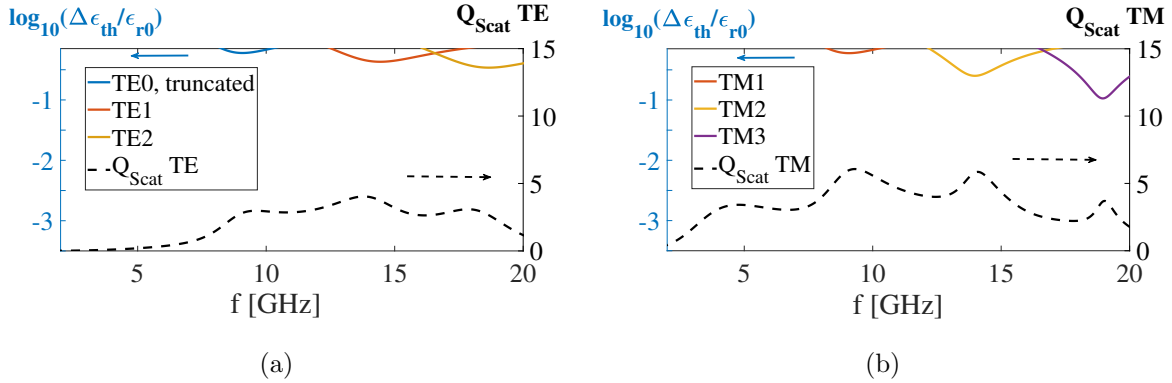


FIG. 3: Threshold values of the modulation strengths $\Delta\epsilon_{th}$ for parametric resonances ($\epsilon_{r0} = 6$, $R = 5$ mm, modulation frequency always satisfies $f_m = 2f$, colored solid curves, left axes), and scattering efficiencies of cylinders with static relative permittivity $\epsilon_r = 6$ (black dashed curve, right axes). (a) is for TE polarization, (b) is for TM polarization.

Reducing the relative permittivity of a time-invariant cylinder results in broader Mie resonances, shown as the black dashed curves in Fig. 3, referenced to the right axes (TE in (a) and TM in (b)). The radius of the cylinder is unchanged ($R = 5$ mm). The calculated threshold $\Delta\epsilon$ based on the truncated eigenvalue problem for each order l are plotted in different colors in Fig. 3, referenced to the left axes. The higher required threshold modulation strengths are attributed to the decreased quality factor of the Mie resonances, exhibited by the time-invariant reference scatterer. Another interesting case to be considered is for the cylindrical scatterer to have $\epsilon_{r0} < 0$. This applies, e.g., to metallic particles or plasma discharges below the plasma frequency or photo-excited semiconducting particles (although for the accurate study of those cases the dispersion in the material permittivity should also be taken into account). Keeping the radius $R = 5$ mm unchanged, and host medium as free space, $\epsilon_h = 1$, the scattering efficiencies of time-invariant scatterers where $\epsilon_{r0} = -1.2, -1.4, -2$, are shown in Fig. 4(a). The results for the TM polarization are in blue, showing no peaks within the frequency range of interest, and no significant variations as ϵ_{r0} is varied. The TE polarization, on the other hand, shows sharper Mie resonances as $|\epsilon_{r0}| \rightarrow 1$. The absence of sharp resonances for TM waves can be explained based on an analogy to the plasmonic resonances exhibited by, for example, an infinitely long metallic cylinder; localized surface plasmon resonances are not supported if physical boundaries along the direction of the electric fields are lacking, as in our TM case. Taking a further step to consider the time-modulated sys-

tem, choosing $\varepsilon_{r0} = -1.4$, results of the threshold $\Delta\varepsilon$ based on the truncated eigenvalue problem are shown in Fig. 4(b). In this case, parametric resonance is only possible for the TE polarization. What is different from the previous cases with $\varepsilon_{r0} > 0$ is that the mode $l = 0$ is not possible to be parametrically amplified within the frequency range due to a much broader static Mie resonance. Despite this, the minimums of $\Delta\varepsilon$ are close to the Mie resonant frequencies, and the minimum required values decrease for higher order l , showing similar trend to that of the $\varepsilon_{r0} > 0$ case as shown in Fig. 1(a).

IV. MODULATING THE SCATTERING RESPONSE

Superposition of the scattered harmonics of different multipolar modes allows for engineering the field distributions in the far-field range. The magnitude of the electric field of the scattered wave of frequency $f = f^{(0)}$ (under time-modulation $f_m = 2f$), in the farfield range, for a time-modulated dielectric cylinder can be expressed in terms of the Mie scattering coefficients, as

$$\lim_{r \rightarrow \infty} E_{sc}^{(0)}(r, \varphi) = \frac{e^{iq_{h0}r}}{\sqrt{r}} \frac{1}{\sqrt{\pi q_{h0}}} (1 - i) \left[\sum_{l=0}^{\infty} \frac{2}{1 + \delta_{l0}} a_{l+}^{(0)} \cos(l\varphi) \right], \quad (15)$$

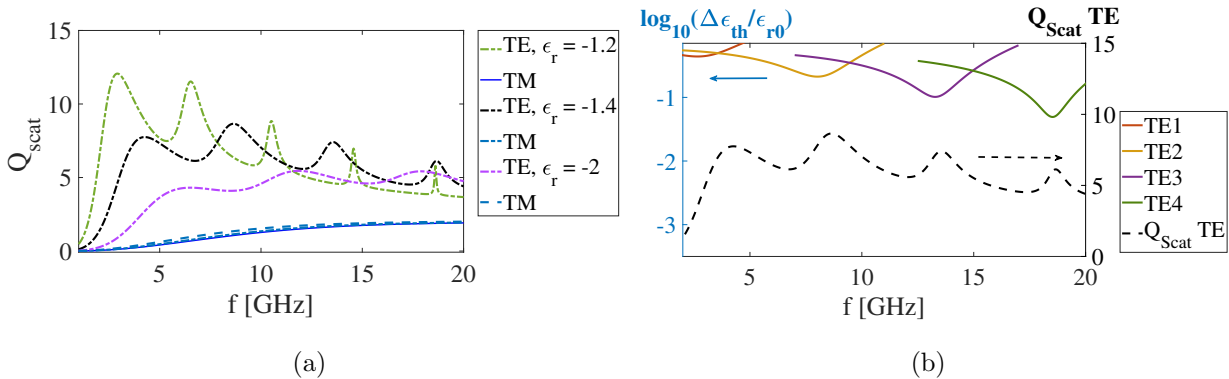


FIG. 4: (a) Scattering efficiencies of static systems $R = 5$ mm, $\varepsilon_{r0} = -1.2, -1.4, -2$ (free-space host medium) of TE (in different colors) and TM (blue, in different line formats) polarizations respectively. (b) Scattering efficiencies the static system, TE polarization, reference property $\varepsilon_{r0} = -1.4$, $R = 5$ mm (black dashed curve, right axes), and $\Delta\varepsilon_{th}$ required for parametric resonances under time-modulation $f_m = 2f$ (colored solid curves, left axes).

where the above expression is for the TE mode, and is in the same form as the expressions in [9] for a static, unmodulated infinite cylinder. With $f_m = 2f$, we have $f^{(1)} = f - f_m = -f = -f^{(0)}$. We consider $n = 0, 1$ as contributing harmonics when evaluating the scattering at the fundamental frequency $f = f^{(0)}$. The magnitude of the electric field of the scattered wave corresponding to the negative-frequency harmonic $n = 1$, is obtained in a similar way by taking the corresponding asymptotic forms of the Hankel functions, given that $q_{h1} = -q_{h0}$ is negative.

$$\begin{aligned} \lim_{r \rightarrow \infty} E_{sc}^{(1)}(r, \varphi) &= \lim_{r \rightarrow \infty} i \sum_{l=0}^{\infty} i a_{l+}^{(1)} \frac{\partial H_l(q_{h1}r)}{\partial(q_{h1}r)} i^l \frac{2}{1 + \delta_{l0}} \cos(l\varphi) \\ &= \frac{e^{iq_{h1}r}}{\sqrt{r}} \frac{1}{\sqrt{\pi q_{h0}}} (-1 - i) \left[\sum_{l=0}^{\infty} \frac{2}{1 + \delta_{l0}} a_{l+}^{(1)} \cos(l\varphi) \right], \end{aligned} \quad (16)$$

$$\text{following from } \lim_{r \rightarrow \infty} \frac{\partial H_l(q_{h1}r)}{\partial(q_{h1}r)} = (-1)^l \sqrt{\frac{2}{\pi q_{h0} R}} \left[\exp[i(q_{h0}r - (l - \frac{1}{2})\frac{\pi}{2})] \right]^*.$$

where the asterisk sign here represents the complex conjugate. The overall electric field, evaluated at f , is the sum of the quantities in Eq. (15) and (16).

An additional degree of freedom in the design arise from the modulation phase β , as mentioned in Eqs. (13) and (14) of Section III, where the truncated approximation was made under parametric resonance conditions. Without assuming the parametric resonance condition, by solving Eqs. (3) and (4) (with $N = 1$ as a simplified example), it can be concluded that only the elements $v_p(n \neq 0)$ of the wave vector gain phase shifts. A more general conclusion is that the modulation phase induces a phase shift of $n\beta$ to the n -th scattered harmonic, as shown by the transfer matrix method in [41].

Following the analytical method in Section II, it is clear that $v_p(n)$, and through them the phase, β , affect the coefficients $\alpha_{l+}^{(n)}$ that determine, among others, the far-field scattering amplitudes. For the scattering at the fundamental frequency $f = f_0$ (under the condition $f_m = 2f$), we have mainly contribution from the scattered harmonics $n = 0, 1$. The corresponding phase shift induced by the time-modulation is then carried over as $\alpha_{l+}^{(n=0)} = (\alpha_{l+}^{(n=0)} | \beta = 0)$, $\alpha_{l+}^{(n=1)} = e^{i\beta} (\alpha_{l+}^{(n=1)} | \beta = 0)$. This can be used to tune the phase difference between $a_{l+}^{(0)}$ and $a_{l+}^{(1)}$ for a certain multipolar order l . The overall radiation pattern may thus be controlled via varying the interference between those coefficients, as shown in the specific numerical examples discussed below.

An example where we excite both the zeroth and first order ($l = 0, 1$) TE modes, under

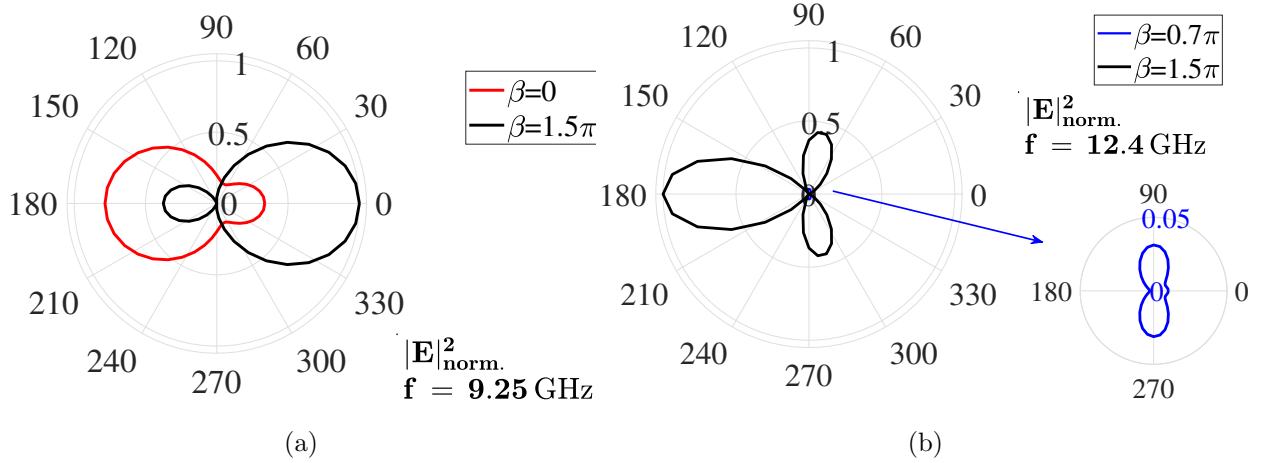


FIG. 5: Field distribution $|E|^2$, in the plane normal to the cylindrical axis, for a cylinder of periodically time modulated permittivity and $\varepsilon_{r0} = 12$, $R = 5$ mm. (a) The field is evaluated at $f = 9.25$ GHz (under $f_m = 2f$), for $\Delta\varepsilon = 8.2$, $N = 3$. Two cases shown: $\beta = 0$ in red, and $\beta = 1.5\pi$ in black. The field is normalized to the maximum value for the $\beta = 1.5\pi$ case. (b) The field is evaluated at $f = 12.4$ GHz, for $\Delta\varepsilon = 5.5$, $N = 3$. $\beta = 1.5\pi$ in black, and $\beta = 0.7\pi$ in blue, with a zoom-in inset showing the distribution on a much smaller scale. Both are normalized to the maximum of the $\beta = 1.5\pi$ case.

modulation conditions for $\Delta\varepsilon$ close to but slightly below those for the parametric resonances (to obtain finite parametric amplification instead of the parametric oscillation regime which is limited by pump depletion in practice), is shown in Fig. 5(a). The calculation for the scattering coefficients is carried out with $N = 3$ (as required for high $\Delta\varepsilon$, shown in Fig. 1(a)). The incident frequency is $f = 9.25$ GHz (under modulation frequency $f_m = 2f = 18.5$ GHz), and the modulation strength $\Delta\varepsilon = 8.2$, which is below the threshold modulation strength corresponding to the intersection of the blue and red dots in Fig. 1(a) (close to 9.25 GHz). The radiated power intensity is plotted as $|E|^2$, evaluated at $f^{(0)} = f$. Field distribution at this frequency contains contributions from the two scattered harmonics $n = 0$ and $n = 1$. If the phase of the applied time-modulation is $\beta = 0$ (red), predominantly backward radiation is obtained from the calculations, while $\beta = 1.5\pi$ (black) gives predominantly forward radiation. The field distribution is normalized by the maximum of the field at $\beta = 1.5\pi$. The field strengths for both cases are strong, due to parametric amplifications. The induced phase difference allows for the switching of the radiation main lobe at the

same evaluation frequency $f = f_m/2$, through varying the phase β of the time-modulation. Distinct from the previous work for spherical particles [36], here one can switch between two contrasting regimes very easily without redesigning the scattering particle.

If, instead, the electric dipole and quadrupole moments ($l = 1, 2$) are excited simultaneously, at Floquet frequency $f = 12.4$ GHz ($f_m = 24.8$ GHz), and $\Delta\varepsilon = 5.5$, the resultant farfield distribution is shown in Fig. 5(b). When $\beta = 1.5\pi$ (black), the main lobe is in the backward direction. The conditions for suppressing forward scattering (or backward scattering, in the example of Fig. 5(a)) are discussed in the Appendix D). For $\beta = 0.7\pi$, the field distribution is not visibly clear when plotted on the same scale (blue), but its strength (normalized to the maximum of the field at $\beta = 1.5\pi$) is reduced by around 20 times as shown in the inset. At $\beta = 0.7\pi$, there is destructive interference between the two harmonics, resulting in the cancellation of the fields. Here the induced phase due to the time-modulation allows for ‘switching off’ the far-field.

Although we considered lower-order modes that lead to relatively high modulation strengths required for exciting different modes simultaneously, one will be able to significantly decrease the required modulation strengths to practical values by switching to higher order modes. This is not considered in the current work as our purpose is to explore and demonstrate theoretically the role of the modulation phase.

V. CONCLUSIONS

We have developed an analytical framework combining Floquet and Mie theories for evaluating the scattering by an infinitely long cylindrical scatterer with periodically time-modulated, non-dispersive permittivity. Applying this framework, we identified, among others, the threshold modulation strengths required to trigger parametric Mie resonances, demonstrating that the required modulation strength is directly related to the quality factor of the corresponding Mie resonances in the static system. Our analysis further reveals that, beyond scattering enhancement, the far-field radiation pattern in the presence of multiple multipolar modes can be dynamically controlled through the modulation phase. In particular, we demonstrated the possibility of either dynamically switching the directions of the main radiation lobes or completely suppressing the far-field radiation, solely by varying the modulation phase.

Our study constitutes a comprehensive investigation of time-modulated cylindrical scatterers, highlighting their strong potential for the realization of time-modulated metamaterials and metasurfaces. Furthermore, it underscores the critical role of the modulation phase in multimode time-periodic systems, as the modulation phase governs the interference among the different modes and thus enables complete reconfiguration of the scattered-field profile.

Possible future directions include extending the analysis to cylinders with dispersive time-modulated permittivity, a configuration that could be experimentally realized, for example, using plasma discharge tubes [42], where the plasma frequency can be periodically tuned in time through external excitation sources.

ACKNOWLEDGMENTS

This work was supported by the European Union under the call “EIC Pathfinder Open 2022” (Project PULSE, project no. 101099313).

-
- [1] G. Ptitsyn, M. S. Mirmoosa, and S. A. Tretyakov, “Time-modulated meta-atoms,” *Physical Review Research* **1**, 023014 (2019).
 - [2] C. Caloz and Z.-L. Deck-Leger, “Spacetime metamaterials—part ii: Theory and applications,” *IEEE Transactions on Antennas and Propagation* **68**, 1583–1598 (2019).
 - [3] Z. Wu and A. Grbic, “Serrodyne frequency translation using time-modulated metasurfaces,” *IEEE Transactions on Antennas and Propagation* **68**, 1599–1606 (2019).
 - [4] J. Mendonça and P. Shukla, “Time refraction and time reflection: two basic concepts,” *Physica Scripta* **65**, 160 (2002).
 - [5] V. Pacheco-Peña and N. Engheta, “Temporal aiming,” *Light: Science & Applications* **9**, 129 (2020).
 - [6] S. Taravati and A. A. Kishk, “Space-time modulation: Principles and applications,” *IEEE Microwave Magazine* **21**, 30–56 (2020).
 - [7] M. Lyubarov, Y. Lumer, A. Dikopoltsev, *et al.*, “Amplified emission and lasing in photonic time crystals,” *Science* **377**, 425–428 (2022).
 - [8] E. Galiffi, R. Tirole, S. Yin, *et al.*, “Photonics of time-varying media,” *Advanced Photonics*

- 4, 014002–014002 (2022).
- [9] V. Pacheco-Pena, D. M. Solís, and N. Engheta, “Time-varying electromagnetic media: opinion,” *Optical Materials Express* **12**, 3829–3836 (2022).
- [10] G. Ptitsyn, M. S. Mirmoosa, S. Hrabar, and S. A. Tretyakov, “Time-modulated circuits and metasurfaces for emulating arbitrary transfer functions,” *Physical Review Applied* **20**, 014041 (2023).
- [11] N. Engheta, “Four-dimensional optics using time-varying metamaterials,” *Science* **379**, 1190–1191 (2023).
- [12] F. R. Morgenthaler, “Velocity modulation of electromagnetic waves,” *IRE Transactions on microwave theory and techniques* **6**, 167–172 (1958).
- [13] V. Pacheco-Peña and N. Engheta, “Antireflection temporal coatings,” *Optica* **7**, 323–331 (2020).
- [14] H. Li and A. Alù, “Temporal switching to extend the bandwidth of thin absorbers,” *Optica* **8**, 24–29 (2020).
- [15] M. Mostafa, M. Mirmoosa, E. Galiffi, *et al.*, “Broadband amplification of light through adiabatic spatiotemporal modulation,” *arXiv preprint arXiv:2506.20358* (2025).
- [16] M. M. Asgari, P. Garg, X. Wang, *et al.*, “Theory and applications of photonic time crystals: a tutorial,” *Advances in Optics and Photonics* **16**, 958–1063 (2024).
- [17] X. Wang, P. Garg, M. Mirmoosa, *et al.*, “Expanding momentum bandgaps in photonic time crystals through resonances,” *Nature Photonics* **19**, 149–155 (2025).
- [18] A. C. Valero, S. Gladyshev, D. Globosits, *et al.*, “Resonant states of structured photonic time crystals,” *arXiv preprint arXiv:2506.01472* (2025).
- [19] E. Lustig, O. Segal, S. Saha, *et al.*, “Photonic time-crystals-fundamental concepts,” *Optics Express* **31**, 9165–9170 (2023).
- [20] M. Mostafa, A. Díaz-Rubio, M. Mirmoosa, and S. Tretyakov, “Coherently time-varying metasurfaces,” *Physical Review Applied* **17**, 064048 (2022).
- [21] C. Simovski, M. S. Mirmoosa, M. Sidorenko, and S. Tretyakov, “Electromagnetic time interfaces in wire media: Innovations for subwavelength imaging,” *Physical Review Research* **7**, 033165 (2025).
- [22] P. Garg, A. G. Lampryanidis, D. Beutel, *et al.*, “Modeling four-dimensional metamaterials: a t-matrix approach to describe time-varying metasurfaces,” *Optics Express* **30**, 45832–45847

- (2022).
- [23] N. Chamanara, Y. Vahabzadeh, and C. Caloz, “Simultaneous control of the spatial and temporal spectra of light with space-time varying metasurfaces,” *IEEE Transactions on Antennas and Propagation* **67**, 2430–2441 (2019).
 - [24] S. B. İplikçioğlu and M. Aksun, “Analytical modeling of time-varying and dispersive metasurfaces with surface susceptibility operators,” *Physical Review B* **111**, 245141 (2025).
 - [25] D. Ramaccia, D. L. Sounas, A. Alu, *et al.*, “Phase-induced frequency conversion and doppler effect with time-modulated metasurfaces,” *IEEE Transactions on Antennas and Propagation* **68**, 1607–1617 (2019).
 - [26] L. Stefanini, D. Ramaccia, M. Barbuto, *et al.*, “Time-varying metasurfaces for efficient surface-wave coupling to radiation and frequency conversion,” *Laser & Photonics Reviews* **18**, 2400315 (2024).
 - [27] S. Taravati and G. V. Eleftheriades, “Pure and linear frequency-conversion temporal metasurface,” *Physical Review Applied* **15**, 064011 (2021).
 - [28] X. Wen, X. Zhu, A. Fan, *et al.*, “Unidirectional amplification with acoustic non-hermitian space- time varying metamaterial,” *Communications Physics* **5**, 18 (2022).
 - [29] A. Ranadive, M. Esposito, L. Planat, *et al.*, “Kerr reversal in josephson meta-material and traveling wave parametric amplification,” *Nature Communications* **13**, 1737 (2022).
 - [30] Z. Hayran and F. Monticone, “Beyond the Rozanov bound on electromagnetic absorption via periodic temporal modulations,” *Physical Review Applied* **21**, 044007 (2024).
 - [31] D. L. Sounas and A. Alù, “Non-reciprocal photonics based on time modulation,” *Nature Photonics* **11**, 774–783 (2017).
 - [32] Y. Chen, X. Li, H. Nassar, *et al.*, “Nonreciprocal wave propagation in a continuum-based metamaterial with space-time modulated resonators,” *Physical Review Applied* **11**, 064052 (2019).
 - [33] X. Wang, G. Ptitsyn, V. Asadchy, *et al.*, “Nonreciprocity in bianisotropic systems with uniform time modulation,” *Physical Review Letters* **125**, 266102 (2020).
 - [34] I. Stefanou, P. A. Pantazopoulos, and N. Stefanou, “Light scattering by a spherical particle with a time-periodic refractive index,” *Journal of the Optical Society of America B* **38**, 407–414 (2021).
 - [35] G. Ptitsyn, A. Lampryanidis, T. Karamanos, *et al.*, “Floquet–mie theory for time-varying

- dispersive spheres,” *Laser & Photonics Reviews* **17**, 2100683 (2023).
- [36] V. Asadchy, A. Lampranidis, G. Ptitsyn, *et al.*, “Parametric mie resonances and directional amplification in time-modulated scatterers,” *Physical Review Applied* **18**, 054065 (2022).
- [37] N. Stefanou, I. Stefanou, E. Almpanis, *et al.*, “Light scattering by a periodically time-modulated object of arbitrary shape: the extended boundary condition method,” *Journal of the Optical Society of America B* **40**, 2842–2850 (2023).
- [38] D. Globosits, P. Garg, J. Hüpfel, *et al.*, “Exceptional points, lasing, and coherent perfect absorption in floquet scattering systems,” *arXiv preprint arXiv:2510.03133* (2025).
- [39] P. Garg, E. Almpanis, L. Zimmer, *et al.*, “Photonic time crystals assisted by quasi-bound states in the continuum,” *arXiv preprint arXiv:2507.15644* (2025).
- [40] C. P. Mavidis, A. C. Tasolamprou, E. N. Economou, *et al.*, “Polaritonic cylinders as multifunctional metamaterials: Single scattering and effective medium description,” *Physical Review B* **102**, 155310 (2020).
- [41] M. M. Salary, S. Jafar-Zanjani, and H. Mosallaei, “Electrically tunable harmonics in time-modulated metasurfaces for wavefront engineering,” *New Journal of Physics* **20**, 123023 (2018).
- [42] H. Conrads and M. Schmidt, “Plasma generation and plasma sources,” *Plasma Sources Science and Technology* **9**, 441 (2000).
- [43] J. A. Stratton, *Electromagnetic theory*, 1941.

APPENDIX

A: Fields in the scattering system of a time-modulated cylinder

We consider plane wave scattering by an infinite cylindrical scatterer made of a time-modulated medium, embedded in a homogeneous host material (of permittivity ε_h and permeability μ_h). The cylinder is assumed parallel to the z -direction and the incident wave propagates along x -direction. We will express the fields in the system in cylindrical coordinates (r, φ, z) , and in terms of the cylindrical vector harmonics \mathbf{n}_l and \mathbf{m}_l . The harmonics \mathbf{n}_l and \mathbf{m}_l can be expressed (in terms of Bessel functions of first kind, J) as

$$\mathbf{n}_l = kJ_l(kr) \cos(l\varphi) \hat{\mathbf{z}}, \quad \mathbf{m}_l = \frac{l}{r} J_l(kr) \sin(l\varphi) \hat{\mathbf{r}} - k \frac{\partial J_l(kr)}{\partial(kr)} \cos(l\varphi) \hat{\boldsymbol{\varphi}}, \quad (17)$$

with k the wavenumber in the medium.

For the case of TE wave scattering (i.e. electric field perpendicular to the cylinder axis), the incident electric field is along the y -direction, and is considered to be

$$\mathbf{E} = e^{-i\omega t} e^{i\mathbf{k}\cdot\mathbf{x}} \hat{\mathbf{y}} = \mathbf{E}' e^{-i\omega t}, \quad (18)$$

where \mathbf{E}' is not dependent on time. The corresponding magnetic field can be obtained from Faraday's law, $\nabla \times \mathbf{E} = i\omega\mu_0\mu_h \mathbf{H}$ (for harmonic waves of the form $e^{-i\omega t}$), as

$$\mathbf{H} = \mathbf{H}' e^{-i\omega t}, \quad \mathbf{H}' = \frac{1}{Z_0} \frac{ck}{\omega\mu_h} e^{i\mathbf{k}\cdot\mathbf{x}} \hat{\mathbf{z}} = \frac{1}{Z_h} e^{i\mathbf{k}\cdot\mathbf{x}} \hat{\mathbf{z}}, \quad (19)$$

with $Z_0 = \sqrt{\mu_0/\varepsilon_0}$ being the wave impedance in free space, $k = k_0 = \omega\sqrt{\varepsilon_h\mu_h}/c$ is the wavenumber in the host material and $Z_h = Z_0\sqrt{\mu_h/\varepsilon_h}$ is the wave impedance in the host material.

In expressing the fields in cylindrical waves we use the useful expansion[43]

$$e^{i\mathbf{k}\cdot\mathbf{x}} = e^{ikr \cos \varphi} = \sum_{l=0}^{\infty} \frac{2}{1 + \delta_{l0}} i^l J_l(kr) \cos(l\varphi). \quad (20)$$

From the above equation one can immediately see that the incident magnetic field \mathbf{H}' can be expanded as

$$\mathbf{H}'(\mathbf{r}) = \frac{1}{Z_h} \sum_{l=0}^{\infty} \frac{2}{1 + \delta_{l0}} i^l J_l(kr) \cos(l\varphi) \hat{\mathbf{z}} = \sum_{l=0}^{\infty} \frac{2}{1 + \delta_{l0}} \frac{i^l}{k} \frac{1}{Z_h} \mathbf{n}_l. \quad (21)$$

In expressing the electric field in terms of the vector harmonics one can use Ampere's law for harmonic waves, i.e. $-i\omega\varepsilon_0\varepsilon_h \mathbf{E}'(\mathbf{r}) = \nabla \times \mathbf{H}'(\mathbf{r})$. Using cylindrical coordinates in the curl evaluation and the above form of \mathbf{H}' , one can obtain

$$\mathbf{E}'(\mathbf{r}) = \frac{i}{\omega\varepsilon_0\varepsilon_h} \frac{1}{r} \frac{\partial H_z}{\partial \varphi} \hat{\mathbf{r}} - \frac{i}{\omega\varepsilon_0\varepsilon_h} \frac{\partial H_z}{\partial r} \hat{\boldsymbol{\varphi}} = \frac{i}{k} \sum_l \frac{2}{1 + \delta_{l0}} i^l \left[\frac{l}{r} J_l(kr) \sin(l\varphi) \hat{\mathbf{r}} - k \frac{\partial J_l(kr)}{\partial(kr)} \cos(l\varphi) \hat{\boldsymbol{\varphi}} \right]. \quad (22)$$

Thus,

$$\mathbf{E}'(\mathbf{r}) = \mathbf{E}_{\text{inc}}(\mathbf{r}) = i \sum_l \frac{2}{1 + \delta_{l0}} \frac{i^l}{k} \mathbf{m}_l = i \sum_l a_l^0 \mathbf{m}_l, \quad a_l^0 = \frac{2}{1 + \delta_{l0}} \frac{i^l}{k}. \quad (23)$$

with a_l^0 the incident wave expansion coefficients of Eq. (5) of the main text.

For the corresponding magnetic field,

$$\mathbf{H}'(\mathbf{r}) = \sum_{l=0}^{\infty} b_l^{0'} \mathbf{n}_l, \quad b_l^{0'} = \frac{2}{1 + \delta_{l0}} \frac{i^l}{k} \frac{1}{Z_h}, \quad (24)$$

giving $a_l^0/b_l^{0'} = Z_h$.

Given the orthogonality of \mathbf{m} and \mathbf{n} vector functions and the cylindrical symmetry of the problem (due to the cylindrical scatterer), an incident wave of the form of Eq. (23) propagating in the plane perpendicular to the cylinder will excite waves inside the cylinder and scattered waves having the same multipolar functional form, i.e. the electric fields will be linear combinations of functions \mathbf{m}_l , as given in Eqs. (6) and (7) of the main text.

Similarly to the incident wave coefficients, for the scattered harmonics with Floquet order n ,

$$\mathbf{H}_{h+}^{(n)}(\mathbf{r}) = \sum_l b_{l+}^{(n)'} \mathbf{n}'_l(q_{hn}, r), \quad (25)$$

$$\mathbf{E}_{h+}^{(n)}(\mathbf{r}) = i \sum_l a_{l+}^{(n)'} \mathbf{m}'_l(q_{hn}, r), \quad (26)$$

and one can show that $a_{l+}^{(n)'}/b_{l+}^{(n)'} = Z_h$, as the scattered waves also propagate in the host medium.

For the fields inside the time-modulated cylinder, expressed as in Eqs. (6) and (7) of the main text, the different Fourier components will have the form

$$\mathbf{E}_c^{(n)}(\mathbf{r}) = i \sum_{p=-N}^N v_p(n) \sum_l a'_{l;p} \mathbf{m}_l(q_p, \mathbf{r}), \quad (27)$$

$$\mathbf{H}_c^{(n)}(\mathbf{r}) = \sum_{p=-N}^N v_p(n) \sum_l b'_{l;p} \mathbf{n}_l(q_p, \mathbf{r}). \quad (28)$$

It also holds that

$$\nabla \times \mathbf{m}_l(q_p, r) = q_p \mathbf{n}_l(q_p, r). \quad (29)$$

For each p, n, l , using the Faraday's law and Eq. (29), we arrive at

$$\begin{aligned} a'_{l;p} \nabla \times \mathbf{m}_l(q_p, r) &= -b'_{l;p} \mu_0 \mu_r (n\omega_m - \omega) \mathbf{n}_l(q_p, r), \\ q_p a'_{l;p} &= Z_0 \frac{\mu_r (\omega - n\omega_m)}{c} b'_{l;p}. \end{aligned} \quad (30)$$

To summarize, we have the following relations between the scattering coefficients: $a_{l+}^{(n)} = a_{l+}^{(n)'}/a_l^0$; $q_p a_{l;p} = b_{l;p} \mu_r 2\pi(f - nf_m)/c$, $a_l^0 = \sqrt{\mu_h/\varepsilon_h} b_l^0$ and $a_{l+}^{(n)} = \sqrt{\mu_h/\varepsilon_h} b_{l+}^{(n)}$ as stated in the main text.

For the TM polarization, the incident magnetic field is in the y direction. The incident electric field, expressed in a similar way to Eq. (3), is

$$\mathbf{E} = \mathbf{E}'(\mathbf{r})e^{-i\omega t}, \quad \mathbf{E}'(\mathbf{r}) = e^{i\mathbf{k}\cdot\mathbf{x}}\hat{\mathbf{z}}, \quad (31)$$

with cylindrical expansion

$$\mathbf{E}'(\mathbf{r}) = \sum_l \frac{2}{1 + \delta_{l0}} i^l J_l(kr) \cos(l\varphi) \hat{\mathbf{z}} = \sum_l \frac{2}{1 + \delta_{l0}} \frac{i^l}{k} \mathbf{n}_l. \quad (32)$$

From Faraday's law, we then have

$$\mathbf{H}'(\mathbf{r}) = -i \sum_l \frac{2}{1 + \delta_{l0}} \frac{i^l}{k} \frac{kc}{Z_0 \omega \mu_h} \mathbf{m}_l. \quad (33)$$

These fields are very similar to the corresponding ones for TE polarization, except for: 1) the constant coefficient i or $-i$ outside the summation, representing the directions of the fields; 2) the exchange of the cylindrical vector harmonics \mathbf{m}_l , \mathbf{n}_l within the summation, again related to the fields directions as we changed polarization.

B: Truncated eigenvalue problem

Taking into account only the two dominant Fourier harmonics, $n = 0, 1$, Eq. (3) in the main text reduces to the truncated eigen-value problem below (\mathbf{E} can be written as E when either TE or TM mode is considered),

$$\begin{pmatrix} (2\pi f/c)^2 \varepsilon(0) & (2\pi f/c)^2 \varepsilon(-1) \\ [2\pi(f - f_m)/c]^2 \varepsilon(1) & [2\pi(f - f_m)/c]^2 \varepsilon(0) \end{pmatrix} \begin{pmatrix} E^{(0)} \\ E^{(1)} \end{pmatrix} = q^2 \begin{pmatrix} E^{(0)} \\ E^{(1)} \end{pmatrix}, \quad (34)$$

where the Fourier coefficients in the time-modulated relative permittivity, (see Eq. (1) of the main text): are $\varepsilon(0) = \varepsilon_{r0}$, $\varepsilon(1) = e^{i\beta} \Delta\varepsilon/2$, $\varepsilon(-1) = e^{-i\beta} \Delta\varepsilon/2$. The eigenvalue problem is then written expressed as

$$\det \left[\begin{pmatrix} (2\pi f/c)^2 \varepsilon_{r0} & (2\pi f/c)^2 e^{-i\beta} \Delta\varepsilon/2 \\ (2\pi(f - f_m)/c)^2 e^{i\beta} \Delta\varepsilon/2 & (2\pi(f - f_m)/c)^2 \varepsilon_{r0} \end{pmatrix} - q^2 \mathbf{I} \right] = 0, \quad (35)$$

with \mathbf{I} being a 2×2 identity matrix. Given that $f_m = 2f$, the above equation leads to

$$\left[q^2 - \left(\frac{2\pi f}{c} \right)^2 \left(\varepsilon_{r0} - \frac{\Delta\varepsilon}{2} \right) \right] \left[q^2 - \left(\frac{2\pi f}{c} \right)^2 \left(\varepsilon_{r0} + \frac{\Delta\varepsilon}{2} \right) \right] = 0. \quad (36)$$

The eigenvectors then follow by inserting the $q_{1,2}$ values from Eq. (36) into Eq. (35), as listed in Section 3 of the main text. The normalization of the eigenvector \mathbf{v}_p does not affect the parametric resonance conditions, which can be shown by writing down the determinant of the 4×4 matrix of Eq. (13) in the main text, and equating it to zero. Any normalization factor to the eigenvectors is carried over as a constant multiplication factor in solving the equation. For a more general case, considering both positive and negative n (e.g. $N = 1$, $n = -1, 0, 1$, without truncation under the parametric resonance condition), the normalization factor to \mathbf{v}_p scales the $a_{l;p}, b_{l;p}$ on the LHS of Eqs. (8,9), which are the scattering coefficients describing the time-modulated material inside the cylinder. Mathematically, this is due to the terms with δ_{n0} on the RHS of the equations, describing a fixed magnitude of the incident waves. In terms of the physical insight, the magnitude of the E field inside the cylinder does not change if we change the normalization factor affecting $v_p(n)$ (as can be seen from Eq. (6)). The normalization factor to the eigenvectors \mathbf{v}_p therefore has no physical meanings.

C: Threshold modulation strengths and Mie resonances

As discussed in [18], parametric resonances are realized when the corresponding complex eigenfrequency of the static resonant system is brought to the real axis upon the periodic modulation. Recall that for the static cylinder, the scattering coefficients are (here it is equivalent to the time-varying model with $N = 0$):

$$\begin{aligned} \text{TE mode: } a_{l+} &= \frac{\sqrt{\mu_h/\varepsilon_h} J_l(qR) J'_l(kR) - \sqrt{\mu_r/\varepsilon_{r0}} J_l(kR) J'_l(qR)}{\sqrt{\mu_r/\varepsilon_{r0}} H_l(kR) J'_l(qR) - \sqrt{\mu_h/\varepsilon_h} J_l(qR) H'_l(kR)}, \\ \text{TM mode: } b_{l+} &= \frac{\sqrt{\mu_h/\varepsilon_h} J'_l(qR) J_l(kR) - \sqrt{\mu_r/\varepsilon_{r0}} J'_l(kR) J_l(qR)}{\sqrt{\mu_r/\varepsilon_{r0}} J_l(qR) H'_l(kR) - \sqrt{\mu_h/\varepsilon_h} H_l(kR) J'_l(qR)}, \end{aligned} \quad (37)$$

for the TE and TM modes respectively. The complex eigenfrequencies for either mode can be evaluated via setting the denominators of the scattering coefficients to 0. The imaginary parts of the complex eigenfrequencies represent losses and are related to the quality factors of the resonance. It is worth noting that the TE0 and TM1 modes not only occur at the same frequency (as proved previously for the static infinite cylindrical scatterers [40]), but they exhibit identical threshold values of the modulation strengths as in the two plots of Fig. 1 in the main text. To relate this observation to the eigenfrequency of the static dielectric cylinder, conditions based on Eq. (37) become, (with $J'_0(qR) = -J_1(qR)$ and $q/k =$

$$\sqrt{\varepsilon_{r0}\mu_r}/\sqrt{\varepsilon_h\mu_h},$$

$$\begin{aligned} \text{TE0} &: \sqrt{\mu_r\varepsilon_h}H_0(kR)J_1(qR) - \sqrt{\mu_h\varepsilon_{r0}}J_0(qR)H_1(kR) \rightarrow 0, \\ \text{TM1} &: \sqrt{\mu_r\varepsilon_h}J_1(qR)H_0(kR) - \sqrt{\mu_h\varepsilon_{r0}}H_1(kR)J_0(qR) \\ &\quad - [\sqrt{\mu_r\varepsilon_h}J_1(qR)H_1(kR)/(kR) - \sqrt{\mu_h\varepsilon_{r0}}H_1(kR)J_1(qR)/(qR)] \\ &\quad \rightarrow 0, \end{aligned} \tag{38}$$

$$\begin{aligned} \text{where we used } J'_l(x) &= J_1(x)/x - J_2(x) \\ &= (J_0(x) - J_2(x))/2, \text{ removing the dependence on } J_2(x) \end{aligned}$$

here the terms within the square bracket of TM1 mode reduces to 0 only if $\mu_r = \mu_h$ (as they are assumed to be both equal to 1 in this work), and this results in the same complex eigenfrequency for the TE0 and TM1 modes, which then explains the same modulation strength required for parametric resonance.

Following the same approach, we can numerically search for the complex eigenfrequencies $f_{\text{eig}} = f_a + if_b$ for each multipolar order l . Based on the Eqns.(20) and (30) in [18], where a sinusoidal modulation scheme in permittivity was also adopted, the modulation threshold is approximately proportional to the ratio of the imaginary part and real part of the eigenfrequency. Therefore, we proceed to investigate the relationship between the minimum modulation threshold (minimum values in Fig. 1, main text, of each solid curve) and the numerically calculated f_b/f_a for each multipolar mode - a linear relationship is found for both TE and TM mode as shown in Figure S.6. The results indicate that the minimum threshold modulation strength is dependent on the losses/quality factors of the eigenmodes of the static system, with an approximate relationship $\Delta\varepsilon_{th}/\varepsilon_{r0} \approx 2/Q$ where $Q = f_a/2f_b$.

D: Suppressing scattering in forward or backward directions

For the case shown in Fig. 5(a) of the main text, the main contributing TE modes are of $l = 0, 1$, and of scattering harmonic order $n = 0, 1$, the using the time-modulation parameters carefully chosen. From Eq. (15) and (16), the forward scattering intensity ($\varphi = 0$) can be expressed as

$$2 \left[e^{-i\pi/4} a_{l=0,+}^{(0)} - e^{i\pi/4} e^{i\beta} a_{l=0,+}^{(1)} + 2 \left(e^{-i\pi/4} a_{l=1,+}^{(0)} - e^{i\pi/4} e^{i\beta} a_{l=1,+}^{(1)} \right) \right]^2, \tag{39}$$

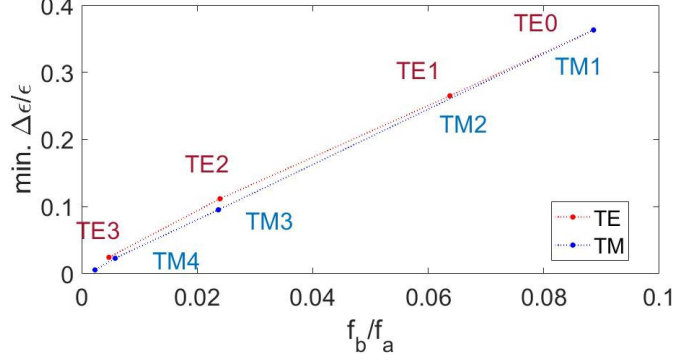


FIG. 6: Minimum points of the threshold modulation strength (linear scale, values from Fig. 1 of main text) against the ratios of imaginary to real parts (f_b/f_a) of the complex eigenfrequencies evaluated for a static cylinder with $\epsilon_r = 12$ and $R = 5$ mm.

whereas the backward scattering intensity ($\varphi = \pi$) is

$$2 \left[e^{-i\pi/4} a_{l=0,+}^{(0)} - e^{i\pi/4} e^{i\beta} a_{l=0,+}^{(1)} - 2 \left(e^{-i\pi/4} a_{l=1,+}^{(0)} - e^{i\pi/4} e^{i\beta} a_{l=1,+}^{(1)} \right) \right]^2. \quad (40)$$

Note that the $a_{l+}^{(n)}$ in the above equations represent coefficients solved at $\beta = 0$, and that the modulation phase β only leads to phase shifts to coefficients of $n = 1$.

For the second case as in Fig. 5(b) of the main text, at 12.4 GHz, the simultaneously excited multipolar orders are of $l = 1, 2$. Therefore we can explicitly write the intensities at $\varphi = 0$ as

$$8 \left(e^{-i\pi/4} a_{l=1,+}^{(0)} - e^{i\pi/4} e^{i\beta} a_{l=1,+}^{(1)} + e^{-i\pi/4} a_{l=2,+}^{(0)} - e^{i\pi/4} e^{i\beta} a_{l=2,+}^{(1)} \right)^2, \quad (41)$$

and at $\varphi = \pi$

$$8 \left(-e^{-i\pi/4} a_{l=1,+}^{(0)} + e^{i\pi/4} e^{i\beta} a_{l=1,+}^{(1)} + e^{-i\pi/4} a_{l=2,+}^{(0)} - e^{i\pi/4} e^{i\beta} a_{l=2,+}^{(1)} \right)^2. \quad (42)$$

Based on the above expressions, we tune the parameter, i.e. β to minimize or maximize the scattering intensity in certain directions.